Model sensitivity analysis of scattering-induced attenuation of ice-coupled waves

L. G. Bennetts[1,*], V. A. Squire

Department of Mathematics and Statistics, University of Otago, P. O. Box 56, Dunedin 9054, New Zealand.

Abstract

The sensitivity of the rate of exponential decay of wave energy through the ice-covered oceans is investigated using a two-dimensional (one horizontal and one depth) linear model. Attenuation in the model results from multiple wave scattering caused by features (irregularities) in the ice cover. The focus of the study is the assimilation of ocean wave / sea ice interactivity — experienced via the attenuation in the model, into an operational ice/ocean forecasting paradigm. Attenuation coefficients are considered, which define the rate of exponential decay as functions of the properties of the ice cover and the incident wave field. It is shown first that wave scattering can be highly sensitive to the values of Young's modulus that are typical of natural sea ice, but that the difference between the values for first-year and multi-year ice is small. Three common ice cover features, namely floes, cracks and pressure ridges, are then examined and compared. Regimes in which particular irregularities are dominant are identified and approximations are derived for the attenuation coefficients produced by each feature. Attenuation produced by rough ice is considered as well, but it is found to be insignificant compared to that due to the three prototype irregularities chosen.

Keywords: Ocean waves, gravity waves, sea ice, ice floes, ice roughness

*Corresponding author. Tel: +61 883133143

Email addresses: luke.bennetts@adelaide.edu.au (L. G. Bennetts), vernon.squire@otago.ac.nz (V. A. Squire)

[1]Current address: School of Mathematical Sciences, University of Adelaide, South Australia 5005, Australia

1. Introduction

The energy associated with ocean surface gravity waves has been observed to attenuate exponentially with the distance it travels, as it permeates deeper into the vast expanses of floating sea ice that encircle the polar regions for much of the year [17, 21]. In this manner, the presence of the sea ice provides a physical defence to the shoreline that reduces the possibility of the coastal reaches of polar and subpolar ice masses, e.g. ice shelves, ice tongues and local icebergs, being damaged as a result of oscillations induced directly, or indirectly via nonlinear wave interactions, by ferocious storms and their associated waves and swell [8, 6]. The phenomenon has recently been brought into focus with the report of the remarkable calving, after 46 years of stability, of 125 km^2 of the Sulzberger Ice Shelf in Antarctica during the summer period of minimum sea ice extent, which is believed to have been assisted by waves dispersing from the tsunami triggered by the Honshu earthquake in Japan over 10,000 km away [7].

The proportion of the wave energy that enters the sea ice expanse causes the sea ice to bend and flex rhythmically as it passes, producing propagating deflections that are known as ice-coupled (or flexural-gravity) waves. Ice-coupled waves impose stresses and strains on the ice that can cause it to break if the waves are sufficiently severe.

Because of the attenuation referred to above, wave-induced fracture is normally confined to a finite distance from the ice edge, i.e. the boundary between the open and ice-covered parts of ocean. This typically structures the ice cover into at least two zones: a belt close to the open ocean, where wave activity is substantial, which contains floes of relatively modest diameter; shielding an inner region of larger floes where the waves have decayed enough that they no longer break the ice or do other damage. The latter ice gradually then becomes quasi-continuous with further distance from the ice edge, where it is colonized by cracks, open and refrozen leads, polynyas and pressure ridges. Ocean currents and winds tend to obfuscate this simple pattern.

Despite the patently strong relationship between ocean waves and sea ice, their interactions are not yet built into operational ice/ocean forecasting models and oceanic general circulation models (OGCMs). This is of particular importance to all maritime endeavours in the polar and subpolar seas, notably in regard to the safety of offshore engineering activities, such as oil exploration, and boats and ships engaged in, e.g. fisheries and geophysical

or hydrographical prospecting. Vital operational forecasts to support these activities are currently incomplete, as they neglect a fundamental physical process that is known to affect the sea ice cover considerably. Moreover, the well-documented reductions in ice thickness, extent and concentration in the summer Arctic Ocean, which have caused the ice to become more akin to sea ice located near the open ocean, suggests that ocean waves will now have a much greater influence than hitherto. In response to this omission, an ice/ocean model was proposed by [9], which couples waves and ice through the fracture and attenuation processes, but only in a single transect of the ocean. An extension to a two-dimensional ocean surface is currently under construction and is expected to lead to assimilation into an OGCM.

Wave scattering is now established as the primary dissipative mechanism that leads to attenuation, at least for the most destructive range of wave periods present. When a wave encounters any 'irregularity' in the ice cover, it is partially reflected and partially transmitted. The accumulation of these scattering events leads to the observed exponential attenuation. The rate of the attenuation is dependent on the properties of the ice cover, e.g. the thickness profile and the surface concentration, and those of the incident wave field, e.g. the wave period. Other mechanisms, such as 'turbulence' in the water between ice floes, the inelasticity of sea ice and floe-floe collisions, also contribute, and are believed to dominate over specific ranges of wavelength.

Modelling the scattering-induced attenuation in a natural expanse of floating sea ice requires the simultaneous calculation of a vast number of scattering events. Efficient and innovative methods to accomplish this have been developed over the last 2–3 decades by a number of different research groups, and the relevant literature is documented in the reviews of [16] and [15]. At present it is possible to model the propagation of waves through a transect of the ice-covered ocean, in which the sea ice contains irregularities such as floe edges, cracks and pressure ridges [4]. An essential component of the current models is the inclusion of randomness (of the wave phase or the geometry), which acknowledges the lack of order in the physical situation being represented mathematically. Three-dimensional models are also available, e.g. [3], although the computational expense they incur is highly restrictive and this remains an area that requires further advances.

In a nutshell the investigation presented here is motivated by the proposed integration of an attenuation model outlined by [4] into the two-dimensional extension of [9]. In the operational model the region of the ice-covered ocean of interest is meshed on a relatively fine scale ($\sim 3.5\,\mathrm{km}$). An incident wave

field is sampled from a surrounding course mesh, which is part of an 'outer' ocean model, and the waves subsequently propagate through the ice-covered region in discrete time. At each time step and within each grid cell the attenuation rate is selected, for the spectrum of waves present, from a look-up table generated by the attenuation model. The attenuation component in the operational model is therefore computationally intensive and its overall success is dependent on the optimization of the call to the look-up table, i.e. the reduction of its dimension. Consequently, it is necessary to eliminate any extraneous information, i.e. given a cell with average ice cover properties and the wave field present, what are the key determinants of the attenuation rate and which ones are less influential? The sensitivity analysis presented in this investigation proposes to help answer this question. It will also provide an insight into the processes underlying scattering-induced attenuation in the ice-covered oceans.

2. A two-dimensional model

In the present study the geometry is restricted to be uniform in one horizontal direction and waves propagate with crests aligned with this plane. There is hence no evolution of the directional spectrum of the waves and no lateral energy leakage. Although three-dimensional models are becoming increasingly sophisticated, see e.g. [3] and [2], it is currently not possible to absorb into them the level of heterogeneity that will form the basis of the present work.

The model assumes waves of small amplitude in relation to their length, so that linear theory may be applied. Under the further assumptions that the fluid is homogeneous, inviscid and in irrotational motion, the fluid's velocity field is described using a scalar, although complex-valued, potential function. For regions in which wave-ice interactions occur, the ocean is usually deep, and its topography is not thought to contribute to the attenuation process. In the results presented in the current work, the fluid depth is set to be 250 m, as this is sufficiently deep that it does not affect the analysis.

It is customary in scattering models to use a thin-elastic plate to simulate sea ice, as this proves to be representative of the material at the strain rates involved and of the deformations and stresses induced in the ice by typical ocean waves. A reduced (effective) elastic modulus is usually used to take into account delayed elasticity. The thin-elastic plate allows the ice to flex with the fluid motion, and wave energy propagates through the coupled system in

the form of flexural-gravity waves. The material properties of the sea ice are defined by its density, here set as $925.5\,\mathrm{kg\,m^{-3}}$, which is nine-tenths of that of the underlying fluid, and its flexural rigidity. The sensitivity to the latter is investigated in § 4.1.

The surface of the fluid domain is either fully or partially covered by sea ice, in the guise of a thin-elastic plate. Surge motion of the ice-cover is considered negligible and its horizontal position is therefore held fixed.

The sea ice itself is infiltrated with irregularities, similar to those found in natural ice cover. Geometrical inhomogeneities are the sources of wave scattering that gradually reduce the intensity of waves travelling through the domain. Three particular features are modelled, these being floes, cracks and pressure ridges. They are depicted in figure 1.

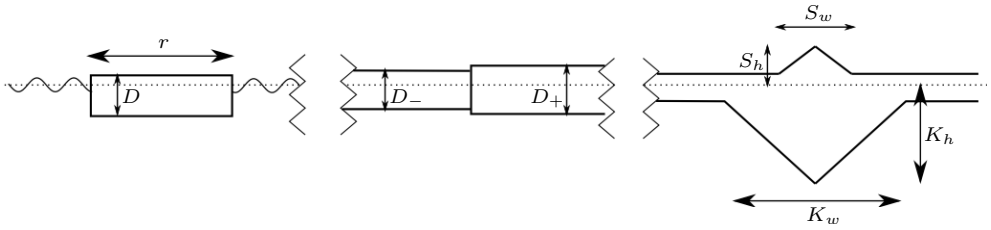

Figure 1: The three features considered. From left to right: a floe, a crack and a pressure ridge.

The feature on the left of figure 1 is a floe. In the present context, a floe is a finite interval (length r) of ice cover, which is separated from any surrounding intervals of ice cover by open water. The thickness of a given floe is set as constant, D, so that scattering is produced by the ice edges alone.

The feature in the middle of figure 1 is a crack. A crack is modelled as a gap between two intervals of uniform ice-cover (i.e. a lead) of zero length. The geometry of a crack thus depends only on the thickness of the surrounding ice cover, D_- on the left and D_+ on the right.

The final feature, on the right of figure 1, is a pressure ridge. The shape of the a pressure ridge used in the present investigation is based on the typical first-year ridge profile calculated by [18]. It is made up of a triangular keel of height K_h and width K_w, and a triangular sail of height S_h and width S_w. The dimensions are related to one another through the identities

$$S_w = 4.3S_h \qquad \text{and} \qquad K_w = 7.5S_h = 2K_h.$$

The thickness of the surrounding ice, D, which is independent of the other dimensions, is here termed the base-level thickness.

In addition to the three features described above, the roughness of the ice cover is included in the model, and is a unique aspect to this investigation [although drag due to bottom roughness of sea ice was recently considered by 11]. The term roughness here describes small-scale variations in the thickness of the ice cover. A numerical solution for rough ice is obtained through a constant panel method, and an example of discretized rough ice is shown in figure 2.

Roughness is thus defined by two parameters. The first is the roughness unit length, λ, which is the width of the panels and is of the order of metres. The second is the roughness amplitude, α, which is the standard deviation of the thickness profile, and is on the order of tenths of metres. The mean thickness is denoted D_0. In the present investigation, the thickness profiles are generated from normal distributions.

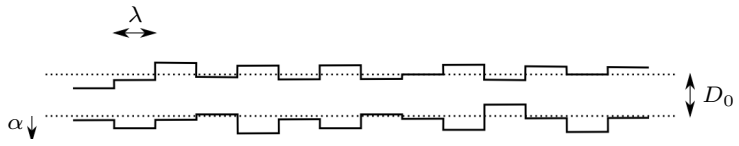

Figure 2: An example of a discretized transect of rough ice.

3. Calculation of the attenuation coefficient

Field measurements of wave activity in the ice-covered regions of the ocean indicate that their attenuation is, at least approximately, exponential [17, 21]. Linear models, such as the one used in this analysis, are certainly able to recreate this property, see e.g. [10]. The quantity of interest is therefore the rate of this exponential attenuation, which is known as the attenuation coefficient and is a quantity that is functionally dependent on wave period and the properties of the ice cover.

An attenuation coefficient is sought for each of the features of the ice cover separately. Given knowledge of the properties of a region of sea ice, the attenuation experienced by a travelling wave spectrum can be estimated as a weighted average of these coefficients [9].

For a particular feature with specified geometrical parameters, the corresponding attenuation coefficient is obtained by populating the model ice

cover with these features. The energy of an incident wave, originating at one spatial extreme, is tracked as it passes through the terrain.

Mathematically, this represents a large multiple scattering problem. Due to the assumption of homogeneity in one spatial direction, it may be solved iteratively. First the scattering properties of the individual features are calculated and are encapsulated in reflection and transmission matrices, noting that evanescent motions may excite motions between features. These matrices are then combined recursively to form reflection and transmission matrices for an increasing number of features, whilst accounting for multiple wave interactions.

Once the scattering matrices have been obtained for the entire transect, the ice-coupled and free-surface wave fields may be constructed by reversing the above procedure. However, it is more stable to recover the attenuation from the transmitted energy, which is derived directly from the transmission coefficients.

In the model it is essential to allow for sufficient randomness in the geometry, in particular positional disorder. An overly idealised geometry leads to coherent interactions and, typically, full transmission, which is not representative of the physical situation. Positional disorder in the model is equivalent to variation of the phase of wave interactions. In the calculation of the attenuation coefficient it is assumed that all phases are equally likely, and results are calculated using Monte Carlo algorithms or ensemble averaging.

For simplicity, in this study the wide-spacing approximation (WSA) method will be invoked, which assumes that wave interactions consist only of the propagating waves. Combined with logarithmic averaging, this allows for the attenuation coefficient to be obtained from knowledge of the average transmission properties of individual features. This is a substantial computational saving and will also be used in the following to gain analytical insight into the attenuation process. In the case of floes the WSA is valid in almost all circumstances, and for cracks and pressure ridges it is valid when features are separated by a distance greater than some lower bound, with the largest value of the lower bound approximately 200 m [see 4]. The WSA is also applied to the floes and cracks themselves.

Because the attenuation coefficient is calculated from the energy transmitted through transects consisting of a chosen number of features, it is natural to obtain an attenuation rate per feature. This is denoted $E = \mathrm{e}^{-\mu\Lambda}$, where E is the transmitted energy, Λ is the number of features and μ is a non-dimensional attenuation coefficient. The WSA therefore produces an

attenuation coefficient μ that is independent of the concentration of features and, for floes, is independent of their length.

An operational model, however, requires a dimensional attenuation coefficient, u say, which is with respect to distance into the ice cover d, and is defined by $E \propto \mathrm{e}^{-ud}$. The attenuation coefficients μ and u are related to one another by the identity

$$u = \mu/d_0.$$

Here d_0 is the average distance between the centres of adjacent features. For floes and pressure ridges $d_0 = l/c$, where l is the average length of the feature (i.e. $l = r$ or $l = K_h$) and c is its average surface concentration. For cracks $d_0 = 1/f$, where f is their frequency of occurrence. It must be noted that the value of d_0 is not related to the distribution of features in the attenuation model, which is independent of such length scales.

The natural attenuation coefficient for roughness is u. It is calculated in a similar fashion to the attenuation coefficient for the other features, although some of the approximations are not valid in this case, so that averaging is necessary and subsequently noise is apparent in the data.

4. Results and analysis

4.1. Young's modulus

In the thin-elastic plate model, the flexural rigidity of sea ice is defined by an effective (i.e. low strain-rate) Young's modulus. There is a significant variation in the recorded values for this parameter. For instance, in their recent review of the engineering properties of sea ice, [19] refer to measurements as low as 1 G Pa and as large as 10 G Pa. Despite the variation it is customary in wave-ice coupled models to use a value of 6 G Pa. Very few investigations of the sensitivity of the scattering model to the Young's modulus have appeared. To the authors' knowledge, the only relevant examples are [14], who studied the variation in the propagating wavenumber as a function of Young's modulus for 1 m thick ice, and [22], who compared the reflection and transmission produced by a crack for a set of thicknesses and Young's moduli.

Here the sensitivity of the model to the value of the Young's modulus is tested using the canonical problem of an ocean wave incident on a single ice edge. The data presented in figure 3 are based on the proportion of the incident wave energy reflected by the ice edge, as a function of wave

period and Young's modulus, for the four thicknesses 0.5 m, 1 m, 2 m and 4 m. The interval 1 G Pa to 10 G Pa is chosen for the Young's modulus, based on the range of values quoted by [19]. Note that the contour values are on a logarithmic scale, and that they denote the ratio of the energy reflected for a particular period and Young's modulus to that for the smallest Young's modulus, i.e. 1 G Pa, at the same period.

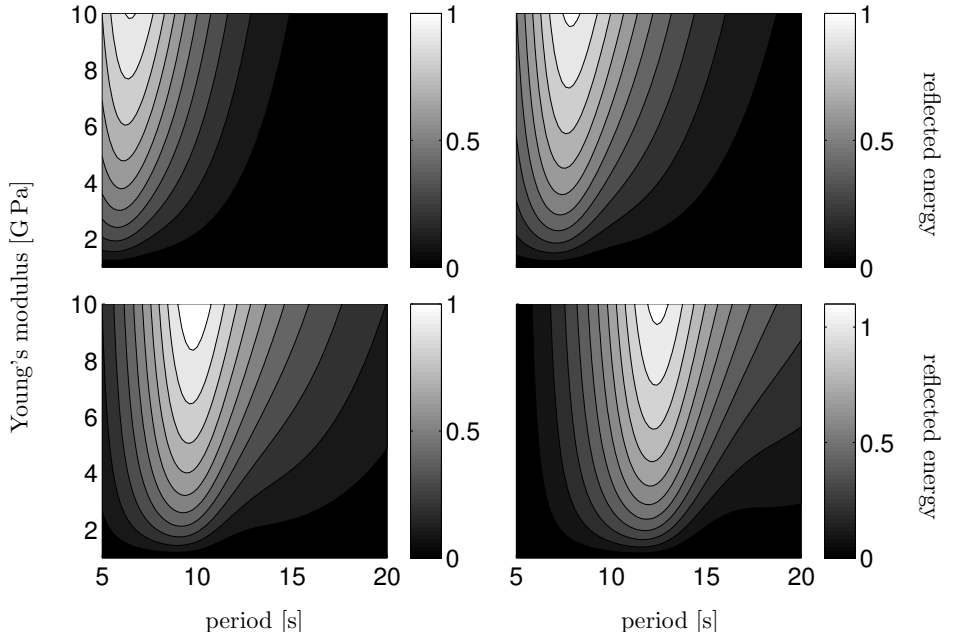

Figure 3: The energy reflected by a single ice edge as a function of wave period and Young's modulus. The contour values at each period are scaled by the values for the smallest Young's modulus in the range considered, i.e. 1 G Pa. The contour values are on a $\log_{10}$ scale. The ice thickness is 0.5 m (top-left panel), 1 m (top-right), 2 m (bottom-left) and 4 m (bottom-right).

It is clear from these results that, for all periods, reflection increases as the Young's modulus becomes larger, which is physically intuitive. The contours display a unique maximum ratio of approximately unit value, and the period at which this maximum is attained increases as the ice becomes thicker, from approximately 6 s to 12 s. Around these periods, reflection therefore changes by approximately an order of magnitude over the range of Young's moduli. However, the sensitivity is far less for larger and smaller periods. For the former this is due to almost all of the wave energy being transmitted regardless of the value of Young's modulus, whereas for the latter, it is because almost

all of the wave energy is reflected in all cases.

An important distinction in sea ice types is between first-year ice and multi-year ice. [19] refer to one set of measurements suggest that first-year ice can have a Young's modulus that is up to 5% greater than its multi-year counterpart. To investigate the significance of this difference, in figure 4 the ratio of the reflection produced by an ice edge for a particular Young's modulus to that for a Young's modulus 10% smaller (i.e. twice the recorded maximum) is shown. The same cases are considered as in figure 3.

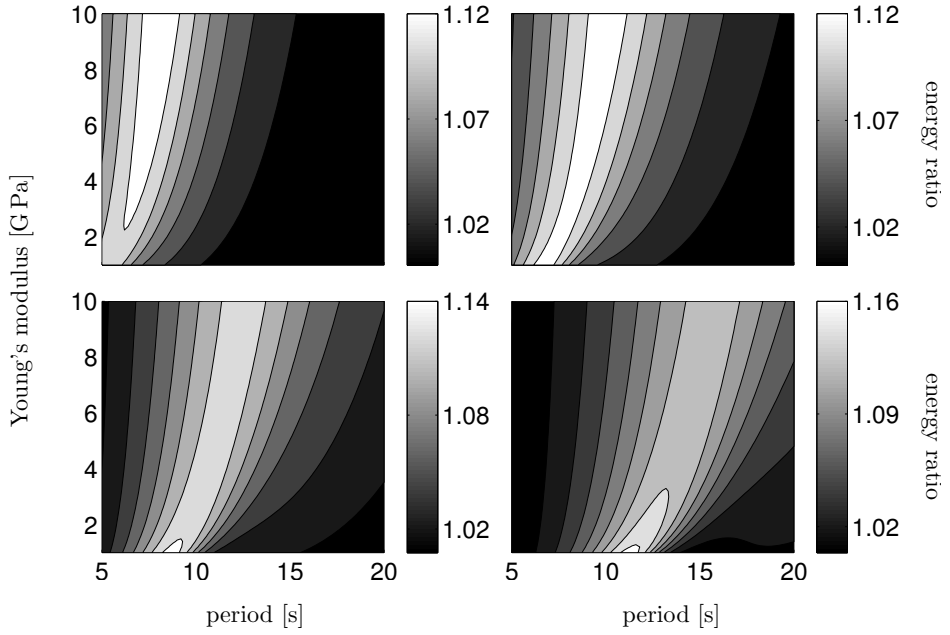

Figure 4: As in figure 3, except that the contours now denote the ratio between the value produced by the indicated Young's modulus and that for a Young's modulus 10% smaller.

The sensitivity is again greatest for the mid-range of periods and moves to larger periods for thicker ice, both being attributes that could be anticipated from the results show in figure 3. However, the differences in the reflections in this case are far smaller than in figure 3, with a maximum ratio here of 14–16%, but usually far less.

It can be concluded from the results shown in this section that reflection can be extremely sensitive to the value of the Young's modulus. This indicates that for application in an operational model it is necessary to carefully select the Young's modulus to match the prevailing ice conditions in

order to capture the attenuation induced by scattering. However, the distinction between first-year and multi-year ice is not in general required. For the remainder of this study the value 6 G Pa will be used for the Young's modulus, as the sensitivities demonstrated for this value are indicative of other admissible Young's moduli.

4.2. Floes

In figure 5 the non-dimensional attenuation coefficient for floes is shown as a function of wave period and ice thickness. The values indicated on the contour plot refer to the base-10 logarithmic order of the attenuation coefficient, which ranges from $O(10^{-7})$ for thin floes at large periods, to $O(10^{0})$ for thick floes at small periods.

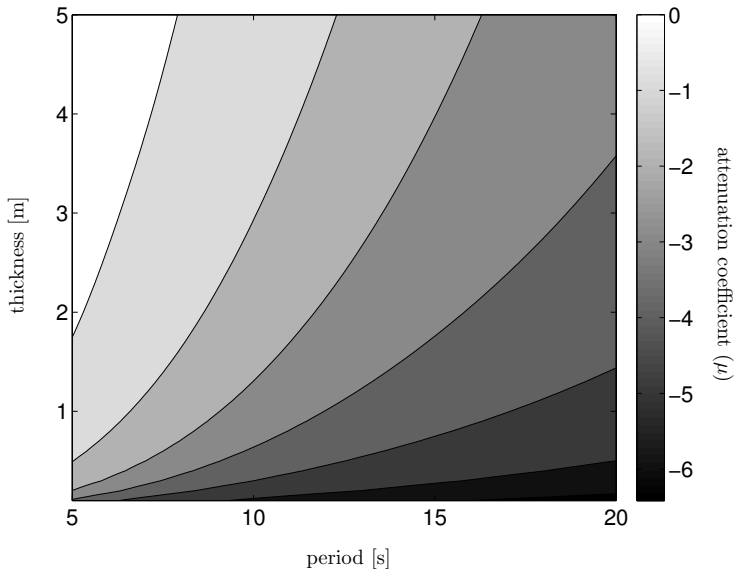

Figure 5: The non-dimensional attenuation coefficient for floes, as a function of wave period and ice thickness. The contour values are on a $\log_{10}$ scale.

Sensitivity of the attenuation coefficient for floes to ice thickness and wave period was identified by [10]. The simple expression derived by [4] for the attenuation coefficient allows for further insight. The expression is

$$\mu = -2\log(1 - \mathcal{R}^2),$$

where $\mathcal{R}^2$ is the proportion of incident wave energy reflected by a single ice edge of a prescribed thickness. Note that no averaging is required to calculate

$\mathcal{R}^2$. It is clear from this expression that the attenuation coefficient tends to infinity logarithmically as reflection becomes full, i.e. $\mathcal{R} \to 1$.

Examination of the reflection, as a function of ice thickness, has shown that it resembles the square of a hyperbolic tangent. In particular, for very thin ice the reflection is negligible but it increases rapidly as the ice becomes thicker, and reaches a unitary asymptote for large thicknesses. An approximation is therefore proposed, namely

$$\mathcal{R} \approx \tanh(a_0 + a_1 D), \tag{1}$$

where D represents the ice thickness. For each wave period, values of the coefficient a_1 and small constant a_0 are determined using a least-squares minimization routine and with 50 equally-spaced points in the abscissa.

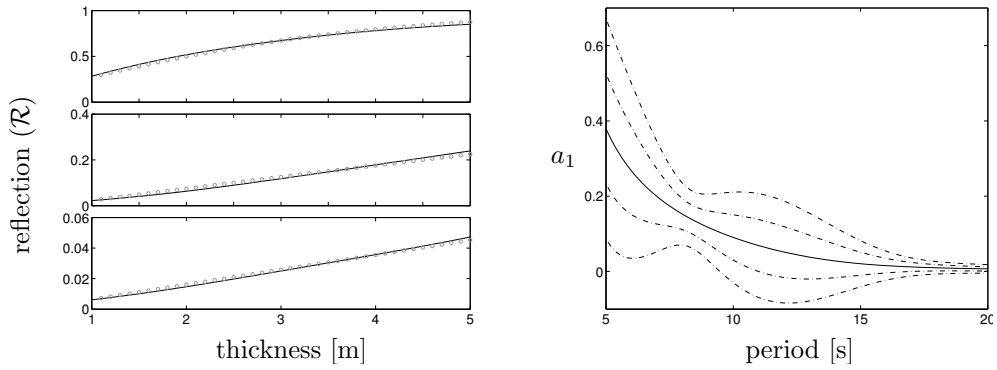

Figure 6: Approximations of the reflection produced by a single ice edge, as a function of ice thickness. The left-hand panels show examples of the reflection as a function of thickness (black curves) and approximations $\tanh(a_0 + a_1 D)$ (grey circles). The wave periods are 6 s (top panel), 12 s (middle) and 18 s (bottom). The right-hand panel is the value of the coefficient a_1 (solid curve), as a function of wave period, and the corresponding 68% and 95% confidence intervals (broken).

Three examples of the reflection coefficient $\mathcal{R}$, as a function of ice thickness, and the corresponding approximations (1) are given in the left-hand panel of figure 6. The right-hand panel of figure 6 shows the values of the coefficient a_1, as a function of wave period, along with the 68% (i.e. one standard deviation) and 95% confidence intervals. It shows that a_1 decreases monotonically with wave period. The pinch in the confidence intervals close to an 8 s wave period is caused by a change in the dominant concavity of the reflection as a function of thickness. It is therefore simply an artefact of approximation (1).

A logarithmic scale for the ordinate axis of the right-hand panel would show that there is a difference of two orders of magnitude between its value at a wave period of 5 s and 20 s. Larger values of a_1 imply that full reflection is attained for thinner ice at that period, and hence that the regime in which the attenuation coefficient grows unboundedly will also exist at this period for a larger range of thicknesses. Consequently the thickness required to achieve a given attenuation will vary by two orders of magnitude over the chosen range of wave periods.

4.2.1. Comparisons with experimental data

Detailed comparisons between scattering-based attenuation models and experimental data on wave attenuation in the ice-covered ocean have been conducted in recent investigations; for example [10, 11] using two-dimensional models and [3] using a three-dimensional model. Reasonable agreement was found between the models and data for central wave periods [estimated as approximately 6 s to 15 s by 10]. But it has also been shown that models tend to underpredict attenuation for large periods and overpredict for small periods. The former is due to the diminished importance of wave scattering as a dissipative mechanism for long waves. Models currently employ an artificial viscosity to simulate the physical processes that dominate in this regime [see e.g. 4]. Inaccuracies for small periods are, at least in part, due to the onset of 'rollover', in which the monotonic increase in attenuation with decreasing period has been observed to reverse below a certain period. One plausible explanation for rollover is the nonlinear transfer of energy from large to small periods [21], but other explanations should also be considered. At present no parameterization of rollover exists in models.

At this juncture it is emphasized that the objectives of the present investigation are to study model sensitivities, and that the comparisons that are made here are not intended for model validation. In particular, no attempt has been made to incorporate additional natural physical processes that will improve the agreement between the model and experimental data in the large and small wave period regimes. Accordingly, the comparison is simply to provide a context for the model sensitivities.

In the field of wave-ice interactions, complete datasets, i.e. power spectra as a function of distance accompanied by recordings of the prevailing ice conditions, are scarce. Indeed two experiments conducted in 1979 are still regarded as the most complete datasets available. The first of these experiments was conducted in the Bering Sea in the spring and is documented

Period [s]	Experimental and model u [1/m] $\times 10^{-4}$	
12.2	0.272 ± 0.054	0.011 – 0.019
9.4	0.438 ± 0.036	0.040 – 0.167
7.6	0.855 ± 0.049	0.149 – 1.201
6.4	1.087 ± 0.037	0.462 – 4.726
5.5	1.214 ± 0.192	1.450 – 12.01

Table 1: A comparison of the (dimensional) attenuation coefficients u recorded in the Bering Sea in 1979 [17] and the attenuation predicted by the model. The model considers only scattering by floes, and the values shown are the upper and lower limits for Young's moduli between 1 G Pa and 10 G Pa.

in [17]. The wave attenuation data recorded during the experiment are accompanied by observations that the approximate ice thickness was 0.5 m and the approximate surface concentration was 0.5. A clear description of the increase in floe diameter with distance into the ice-covered ocean was also given, which identifies three bands of the ice-cover, with average floe lengths 10 m, 25 m and 100 m, respectively. These parameters have been used in the model, with the bands appearing as a weighted average of the attenuation coefficients produced by the three average lengths.

The second experiment was conducted in Kong Oscars Fjord, in north-east Greenland, in the early autumn of 1979. The data obtained during the experiments and details of the prevailing ice conditions are recorded in [21] and [13], respectively. Unfortunately, the account of the latter is not as comprehensive as that of the Bering Sea experiment. Of the two successful experiments that took place during the Kong Oscars Fjord expedition, the first, which was conducted on 4$^{\text{th}}$ September, has the more accurate description of the ice conditions, and is therefore the data used for comparison here. On the 4$^{\text{th}}$ September the concentration was estimated to be 0.3 and the average floe diameter was 65 m. No information on ice thickness was given, so the model uses the value 3.1 m based on a recording in the same location the previous year [as in 10].

Comparisons between the (dimensional) attenuation coefficients predicted by the model and the results of the experiments in the Bering Sea and Kong Oscars Fjord are given in tables 1 and 2, respectively. The experimental data include error bounds from the statistical analysis. Attenuation coefficient intervals are given for the model, ranging from relatively compliant ice with

Period [s]	Experimental and model u [1/m] $\times 10^{-4}$	
14.03	0.29 ± 0.27	0.130 – 0.464
11.88	0.73 ± 0.25	0.268 – 0.818
10.31	1.23 ± 0.19	0.607 – 6.155
9.10	2.01 ± 0.17	1.753 – 10.81
8.14	2.66 ± 0.22	5.501 – 20.22

Table 2: As in table 1 but for the experiment conducted in the Kong Oscars Fjord on the 4^{th} September 1979 [21, 13].

Young's modulus 1 G Pa to relatively rigid ice with Young's modulus 10 G Pa.

The comparison to the Bering Sea experiment in table 1 clearly shows the trends discussed at the beginning of the subsection. For periods 6.4 s and 7.6 s the experimental data fall in the range of the model predictions. For the largest two periods, 9.4 s and 12.2 s, the model underpredicts the observed attenuation, with predictions for all rigidities being an order of magnitude too small in the case of the largest period. For the smallest period the model overpredicts the attenuation in comparison to the experimental data. This overprediction is up to an order of magnitude. Note that rollover is not present in the experimental data here.

Reference to table 2 shows that the model predictions are in better agreement with the experimental data obtained from Kong Oscars Fjord. In particular, the experimental values for the attenuation coefficient lie in the range of the model predictions for all wave periods except for 8.14 s. However, the tendency for a greater sensitivity of the model to wave period is again in evidence. Despite the better agreement seen in this case, no new inferences regarding the capabilities of the model should be drawn from the comparisons. The additional physical processes discussed above, as well as the extension to a fully three-dimensional analysis, remain as key areas for improvement of the model. The comparisons provide further evidence of the importance of the rigidity of the ice in the model.

4.3. Cracks

The scattering properties of cracks are distinguished by a point of full transmission, which is smoothed away by the averaging process, although it remains visible [4]. This characteristic is manifest as a shallow minima in

the attenuation coefficient for cracks. It marks the transition between two regimes, with mass dominating in one and flexure in the other.

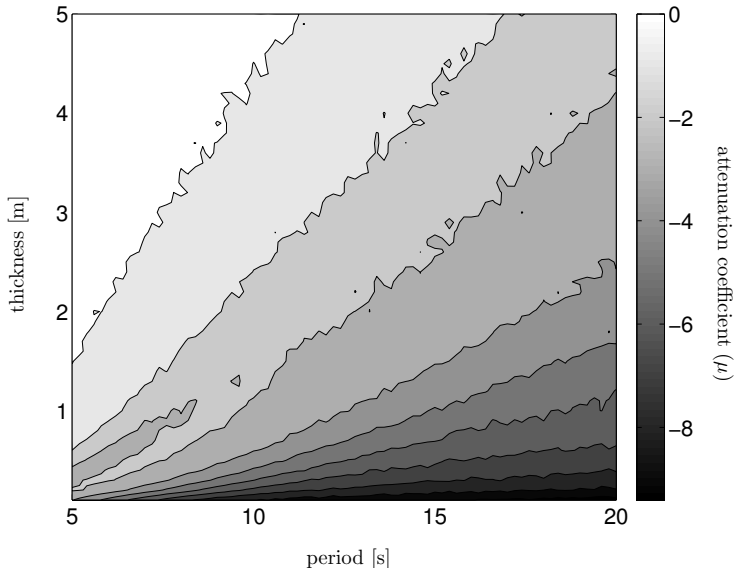

Figure 7: The non-dimensional attenuation coefficient for cracks, as a function of wave period and average ice thickness. The contour values are on a $\log_{10}$ scale.

In figure 7 the attenuation coefficient for cracks is shown as a function of its two determinants, these being wave period and average ice thickness. The thicknesses on either side of the crack are chosen randomly from identical normal distributions, with a standard deviation one-third of the mean value. The results represent the average of 50 simulations, and the noise visible in these results is a by-product of the averaging process.

The trends of the attenuation for cracks are similar to those for floes seen in figure 5, with attenuation increasing for smaller wave periods and larger ice thicknesses. Note that the domain over which the attenuation coefficient is of unit order is larger for cracks than floes, and that the range of cracks extends two orders of magnitude lower than that of floes. The shape of the contours dividing the orders of magnitude of the attenuation coefficient also differs between floes and cracks, being roughly quadratic for the former and linear for the latter.

Due to the presence of two regimes in the results for cracks, it is difficult to simplify the expression for the attenuation coefficient. However, an adequate

approximation was found to be

$$\mu \approx b_0 D^{b_1},$$

where b_0 and b_1 are coefficients that are constant for each individual wave period, and are obtained through a minimization process.

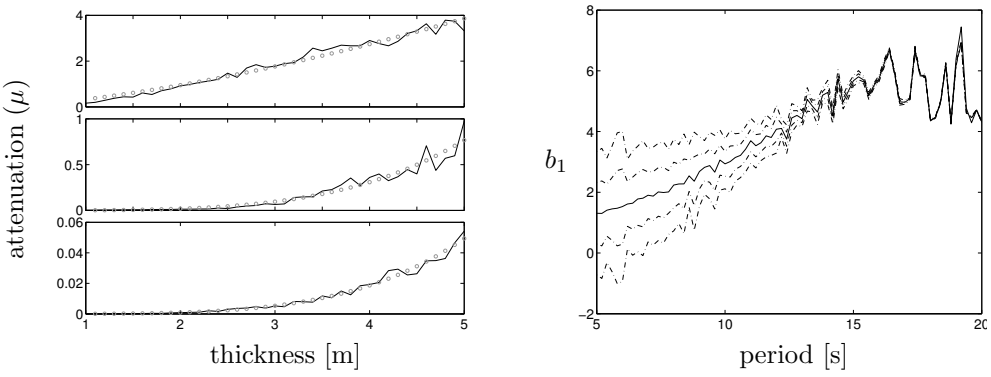

Figure 8: Approximations of the attenuation coefficient for cracks, as a function of ice thickness. The left-hand panels show examples of the attenuation coefficient as a function of thickness (black curves) and approximations $b_0 D^{b_1}$ (grey circles). The wave periods are 6 s (top panel), 12 s (middle) and 18 s (bottom). The right-hand panel is the value of the coefficient b_1 (solid curve), as a function of wave period, and the corresponding 68% and 95% confidence intervals (broken).

Results analogous to those of figure 6 for floes are given for cracks in figure 8. The coefficient b_1 is shown in the right-hand panel along with the corresponding 68% and 95% confidence bounds. It is not monotonic with wave period. Instead, it rises rapidly with increasing wave period from 5 s, until around 10 s, and then fluctuates. The noise visible for larger periods is caused by the sensitivity of the attenuation in this regime, due to the diminished effect of scattering.

A larger value of b_1 clearly indicates greater sensitivity of the attenuation coefficient to ice thickness. The results therefore predict maximum sensitivity for wave period greater than approximately 10 s, and generally smaller variations of the attenuation coefficient with respect to thickness for small periods than large periods.

4.4. Pressure ridges

Despite the restriction to a single profile (first-year type, see § 2), pressure ridges still possess the most parameter dependencies of the features

considered in this study. The attenuation produced by ridges will depend firstly on the incident wave period and the ice thickness within which they are embedded, i.e. the base-level thickness. But it will also depend on the dimensions (width and height) of the ridge. In a forecasting model, it is currently not possible to get details on the dimensions of ridges, and it is therefore particularly important to know their sensitivity.

The profile used (shown on the right-hand side of figure 1) only requires that one of the dimensions is specified, and here the width is chosen, i.e. the keel width K_w. Note that the base-level thickness must also be specified. In the following analysis the widths used will be in the range 20 m to 120 m, and the base-level thicknesses in the range 1 m to 5 m. For large base-level thicknesses and narrow ridges, the width-height formulae become invalid (inverting the keel), although this does not occur for the ranges considered.

Examples of the attenuation coefficient produced by ridges, as a function of ridge width are shown in the left-hand panels of figure 9. The three panels show results for wave periods 6 s (top panel), 12 s (middle) and 18 s (bottom), with the base-level thickness set as 2 m in all cases. As expected, attenuation increases as the ridge becomes wider, and less attenuation is produced for larger periods.

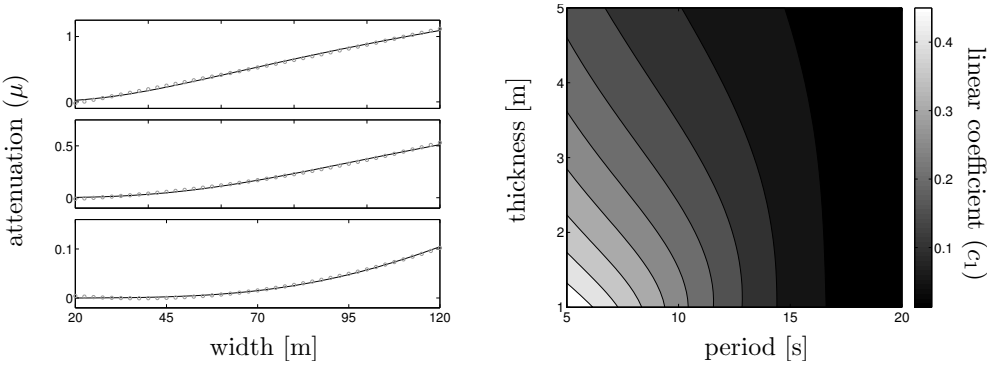

Figure 9: Approximations of the non-dimensional attenuation produced by ridges with respect to their width. The left-hand panels show examples of the attenuation coefficient as a function of ridge width (black curves) and quadratic approximations (grey circles). The wave periods are 6 s (top panel), 12 s (middle) and 18 s (bottom). The base-level thickness is 2 m in all cases. The contours in the right-hand panel show the value of the coefficient of the linear term in the approximation as a function of wave period and base-level thickness.

The attenuation coefficients as functions of ridge width are well approx-

imated by quadratic polynomials, shown by the grey circles. These are calculated using a least-squares minimization routine, and are of the form

$$\mu \approx c_0 + c_1 w + c_2 w^2,$$

where w is the ridge width. In this approximation, the linear term is generally dominant, although the constant term is usually of the same order of magnitude. The coefficient c_1 is therefore deemed to give the best representation of the sensitivity of the attenuation to ridge width. The right-hand panel of figure 9 shows the value of this quantity as a function of wave period and base-level thickness. It is evident from these results that the sensitivity evolves smoothly from being greatest at small periods and small base-level thicknesses to being relatively insensitive at large periods.

An analogous study of the sensitivity of ridges to base-level thickness is given in figure 10. The examples in the left-hand panels are for ridge widths of 25 m (top panel), 50 m (middle) and 100 m (bottom), with all using a wave period 12 s. The trends shown are for larger attenuation when the base-level thickness is small.

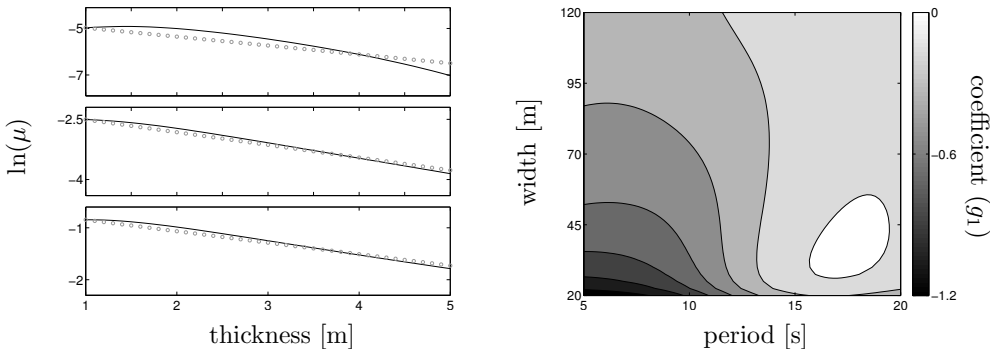

Figure 10: Approximations of the non-dimensional attenuation produced by pressure ridges with respect to base-level thickness. The left-hand panels show examples of the attenuation coefficient as a function of ridge width (black curves) and exponential approximations (grey circles). The ridge width is 25 m (top panel), 50 m (middle) and 100 m (bottom). The wave period is 12 s in all cases. The contours in the right-hand panel show the coefficient g_1 of the exponential approximation as a function of wave period and ridge width.

Simple exponential approximations, of the form

$$\mu \approx g_0 \mathrm{e}^{g_1 D},$$

Period [s]	Exp. u [1/m] $\times 10^{-4}$	Model u [1/m] $\times 10^{-4}$		
12.2	0.272 ± 0.054	0.016	0.016	0.018 – 0.077
9.4	0.438 ± 0.036	0.103	0.129	0.143 – 0.653
7.6	0.855 ± 0.049	0.677	0.945	0.921 – 2.753
6.4	1.087 ± 0.037	2.891	3.162	3.500 – 6.867
5.5	1.214 ± 0.192	8.140	8.295	9.147 – 13.90

Table 3: Comparisons of the (dimensional) attenuation coefficients u calculated during an expedition in the Bering Sea in 1979 (described in § 4.2.1) and the attenuation predicted by the model. Three predictions are made using the model: attenuation due to floes only (left); attenuation due to floes and cracks (middle); and attenuation due to floes and pressure ridges (right). In the latter case an interval is given corresponding to ridges of widths 10 m to 20 m.

for the attenuation coefficient as a function of base-level thickness, are shown by the grey circles. These are not of high accuracy in all circumstances, in particular for large periods and narrow ridges, but they do provide a good representation of the sensitivity of the attenuation to base-level thickness. The value of the coefficient g_1 is given in the right-hand panel of figure 10 across the chosen range of wave periods and ridge widths. It can be inferred that sensitivity is greatest for small periods and narrow ridge widths, and is least for large periods. However, in this case there is more structure in the contours, and, in particular, there is a combination of periods and widths, centred around 18 s and 40 m, respectively, for which attenuation is virtually insensitive to the base-level thickness.

4.4.1. Comparisons with experimental data

Descriptions of prevailing ice conditions to accompany wave attenuation data, are, at best, limited to information on an average floe length, ice thickness and surface concentration. No attenuation experiment currently exists with observations regarding the existence and/or frequency of cracks and pressure ridges. Consequently, whilst it is informative to test how the addition of attenuation due to cracks and ridges affects model-data comparisons, no claim is made regarding an improved representation of the ice cover.

Table 3 shows a second comparison of the attenuation coefficients predicted by the model with the data collected during the 1979 Bering Sea experiment. Three different predictions are taken from the model. The first

is the attenuation produced by floes alone, the second is the attenuation produced by floes and cracks combined, and the third is the attenuation produced by floes and pressure ridges combined. Cracks and ridges are assumed to only exist in the inner band observed during the experiment, in which the floes are approximately 100 m in length. (It is noted that it can equally be the outer band of the ice-cover that is the most heavily deformed depending on the location, season and recent wave activity.) The predictions are based on one crack or ridge per floe in this band. Only small ridges are used, of widths 10 m to 20 m, and, the range of attenuation coefficients corresponding to these widths is presented.

The Young's modulus used for the model predictions is 6 G Pa in all cases. The attenuation coefficients for floes only are therefore contained in the intervals shown in table 1. It is unsurprising then that the agreement with the experimental data is reasonable for the mid-range of periods, 6.4 s to 9.4 s, underpredicted for the largest period, 12.2 s, and overpredicted for the smallest period, 5.5 s. Incorporating attenuation produced by cracks or ridges, of course, increases the attenuation coefficient. The significance of the increase varies depending on the wave period and the particular feature. It can be seen that ridges generally produce larger attenuation than cracks, and that the width of the ridges considered is an important factor. Comparative sensitivities of the features are investigated in detail in § 4.6.

4.5. Roughness

In addition to dependence on mean thickness and wave period, the attenuation produced by roughness, as defined in § 2, varies according to its prevailing amplitude and unit length. Such properties of the ice are correlated with its type, i.e. first-year or multi-year; deformed or undeformed [12].

Numerous data sets exist for the roughness amplitude of sea ice, in both the Arctic and Antarctic [see e.g. 1, 5]. The ranges used in the following analysis are guided by these recordings. Note that the roughness amplitude is here considered independently of pressure ridges. Classical methods for sampling the roughness of sea ice are in-situ drilling and upward pointing submarine sonar. However, reliable images of the underside of sea ice are now possible from autonomous underwater vehicles [20], which promise more comprehensive maps of the ice terrain.

The use of a unit length for roughness in this work is a computational artifice, which is necessary for the investigation. To the authors' knowledge

no data for this quantity are available or any clear means for estimating its value. The values used are therefore commensurate with the resolution of typical experimental recordings of ice properties, and the sensitivity of the attenuation coefficient to this quantity will be established. It is emphasized that a very small unit length in the wave scattering model, which the present investigation is based on, will result in negligible attenuation, and other mechanisms, such as drag, are expected to become dominant [11].

In figure 11 examples are given to demonstrate how the attenuation produced by roughness depends on the roughness amplitude (left-hand panels) and unit length (right-hand panels). (Recall that the natural attenuation coefficient for roughness is per meter, i.e. u.) Each data point is calculated from the average of 100 simulations, in which each simulation consists of 150 thickness variations.

Results are shown for three wave periods, namely 6 s, 12 s and 18 s. The mean thickness is set as 2 m, which is a typical value found in regions of wave-ice interactions, and the behaviours observed are consistent with other thicknesses in the range considered in this investigation. Note that, in the left-hand panel the square-root of the attenuation coefficient is displayed.

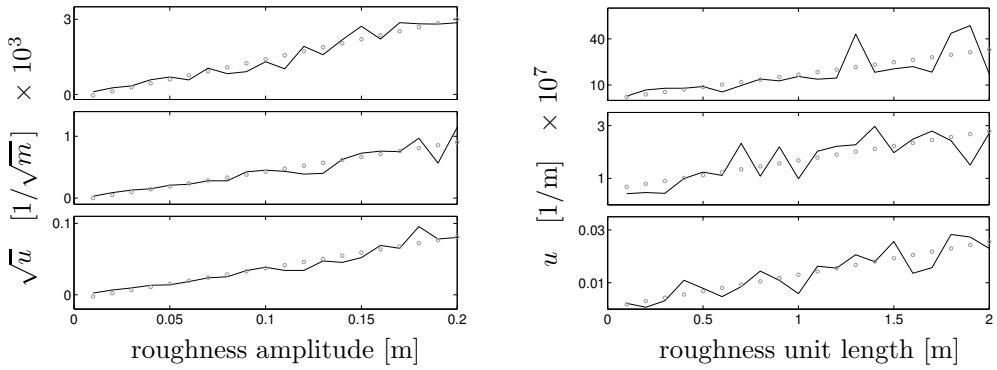

Figure 11: Approximations of the dimensional attenuation produced by roughness with respect to its amplitude and unit length. The left-hand panels show examples of the square-root of the attenuation coefficient, as a function of roughness amplitude (black curves) and the quadratic approximations (grey circles). The right-hand panels show examples of the attenuation coefficient, as a function of roughness unit length (black curves) and the linear approximations (grey circles). The wave period is 6 s (top panels), 12 s (middle) and 18 s (bottom). For the left-hand panels the roughness length is set as 1 m, and for the right-hand panels the roughness amplitude is set as 0.1 m. The mean thickness is 2 m in all cases.

It is clear that the rate of attenuation increases with a larger roughness

amplitude and a greater unit length. Both of these traits are to be expected. Attenuation will continue to grow with increasing amplitude until full reflection is attained. With respect to unit length, the rate of attenuation will begin to decrease in inverse proportion to the length, after a certain, period dependent, limit.

The scale chosen for the ordinate axes illustrates that, in the chosen ranges, the dependence of attenuation to amplitude is approximately quadratic, and to length is approximately linear. This immediately indicates that attenuation is more sensitive to the amplitude of roughness than its unit length. It also follows that the attenuation rate for a particular unit length is representative of the average over a distribution of unit lengths, of which it is the mean value.

Approximations $u \approx (h_0 + h_1\alpha)^2$ and $u \approx j_0 + j_1\lambda$ are therefore sought for the dependence of the attenuation to roughness amplitude and unit length, respectively. These approximations are also shown in figure 11, where, as before, the values of f_i and g_i $(i = 0, 1)$ are found through a minimization routine.

The coefficients h_1 and j_1 give information about the sensitivity of the attenuation coefficient and also its magnitude. These values are shown as functions of wave period in figure 12. Results are given for three mean thicknesses, these being 1 m, 2 m and 4 m.

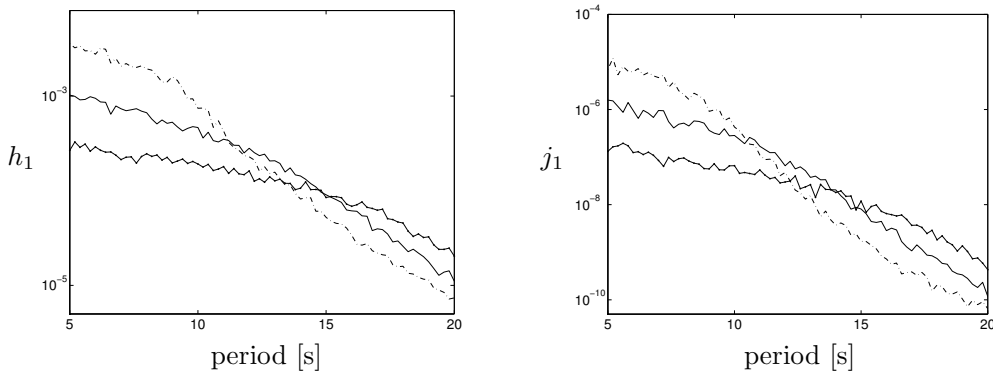

Figure 12: The coefficients h_1 (left-hand panel) and j_1 (right-hand panel) used in the approximations of the attenuation coefficient for roughness, as functions of wave period. Results are given for three mean thicknesses, $D_0 = 1$ m (broken curves), 2 m (solid) and 4 m (dotted).

The qualitative behaviours of the coefficients for amplitude and unit

length are almost identical. Firstly, each of the curves in figure 12 decreases monotonically with wave period. This implies that attenuation is most sensitive to changes in the amplitude and unit length of roughness for small wave periods.

For small periods, the magnitudes of the coefficients are arranged in descending order with respect to increasing mean ice thickness. For large periods the opposite is true, with smaller values of the coefficient for thinner ice. The transition between these two regimes occurs in the period range 10 s to 15 s, approximately. This not only implies that the sensitivity of attenuation to the amplitude and unit length of roughness is greater for thinner ice at small periods and for thicker ice at larger periods, but also that rough ice produces greater attenuation at small periods when the ice is thin, and, conversely, for thick ice at large periods, at a fixed amplitude and unit length.

4.6. Comparative sensitivities

Thus far, the results have established the sensitivities of the attenuation produced by floes, cracks, pressure ridges and roughness to their dependent variables individually. Using this as a basis, attention now switches to the relative sensitivities of the attenuation produced by the different features. This will allow for inferences to be made as to which of the features will dominate the attenuation process in a region of sea ice with known average properties.

In figure 13 the attenuation produced by floes is compared to that produced by cracks (left-hand panel) and pressure ridges (right-hand panel). The contours show the values of the ratio of the relevant non-dimensional attenuation coefficients, as functions of wave period and thickness (base-level in the case of ridges). The ridge dimensions are also a determinant of the attenuation they produce, and here the width is set to the central value of 50 m. The contour values are scaled logarithmically. Therefore, positive values indicate that the attenuation coefficient for floes outweighs that of cracks/ridges, and negative values indicate the opposite.

The left-hand panel, which compares the attenuation coefficients for floes and cracks, illustrates that there are regimes in which either one dominates. Floes cause more attenuation for relatively thin ice and large periods, whereas cracks produce more attenuation for thicker ice (approximately greater than 2 m). The difference is up to 2 orders of magnitude in favour of floes (for periods greater than 15 s and thicknesses less than 0.5 m, approximately), and a single order of magnitude in favour of cracks (for periods greater than

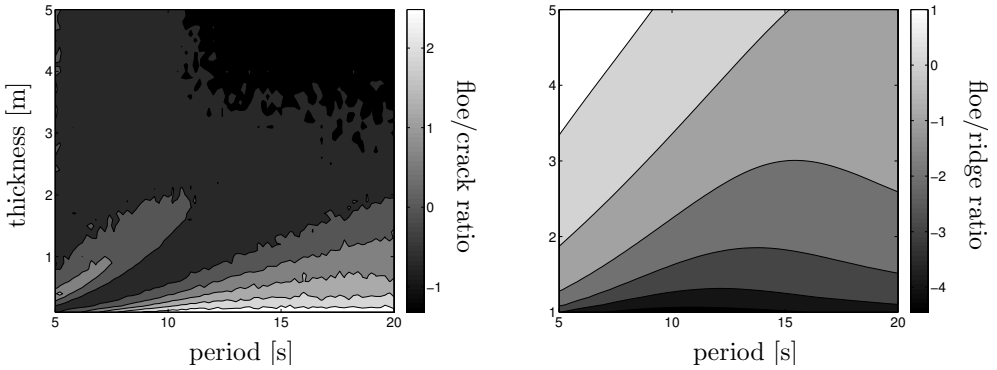

Figure 13: The ratio of the (non-dimensional) attenuation coefficient for floes to cracks (left-hand panel) and for floes to ridges (right-hand panel), as functions of wave period and ice thickness (base-level in the case of ridges). The contour values are on $\log_{10}$ scales.

10 s and thicknesses greater than 3.5 m, approximately). Between these two regimes, in which one feature dominates, the attenuation produced by floes and cracks are comparable, i.e. of the same order of magnitude.

Regimes in which the attenuation coefficient produced by one feature dominates over the other are also displayed, in the right-hand panel, for floes and pressure ridges. However, in this case, floes only dominate for thick (base-level) ice and small periods (greater than 3.5 m and less than 9 s, respectively). Ridges dominate for the majority of the spectrum considered, from thin ice up to a value depending on the wave period, but no less than approximately 2 m. The difference between the attenuation coefficients is also more extreme than for cracks, with that for ridges up to 4 orders of magnitude greater in the chosen range.

As the ratio used for figure 13 is between non-dimensional attenuation coefficients, some additional information must be known to provide physical interpretation. Given an array of floes and an array of cracks with the same average spacing (centre to centre in the case of floes) and ice thickness, the comparison between floes and cracks indicates that

- the floes will produce more attenuation if the ice is thin and the travelling wave has a large period;
- the cracks will produce more attenuation if the ice is thick (approximately greater than 2 m);
- in the intermediate regime, i.e. in many relevant circumstances, the

attenuation rates will be of the same order of magnitude.

Comparing the array of floes to an array of ridges, with the chosen dimensions, and the same spacing (centre to centre), the results indicate that

- the array of ridges will produce far more attenuation in most circumstances;
- the attenuation produced by the array of floes will only match or exceed that of the ridges for thick ice and small wave periods.

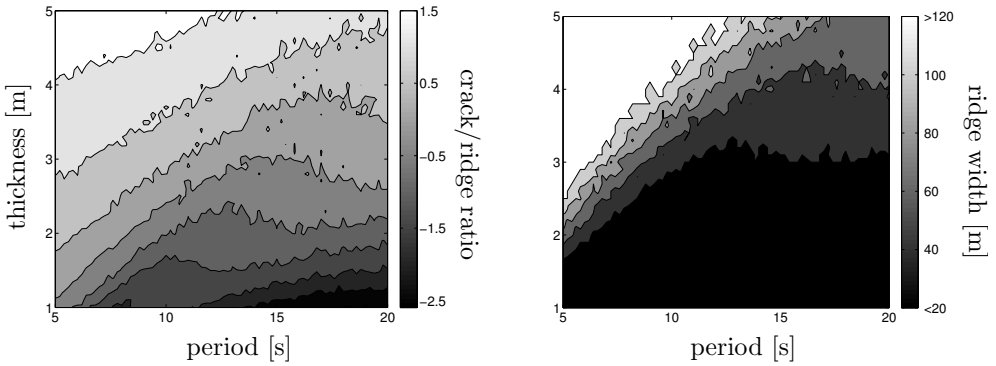

Figure 14: The left-hand panel is the ratio of the (non-dimensional) attenuation coefficient for cracks to ridges, as a function of wave period and ice thickness (base-level for ridges). The contour values are on a $\log_{10}$ scale. The right-hand panel is the width of a ridge required for its attenuation coefficient to exceed that of cracks, as a function of wave period and ice thickness.

The left-hand panel of figure 14 is a corresponding comparison of cracks and ridges, with the width of the latter, as before, 50 m. Again, the attenuation coefficient for ridges dominates for the majority of the spectrum, with the crack attenuation coefficient only becoming of comparable or of greater magnitude for thick ice and small periods. However, the extent to which the attenuation coefficient for ridges exceeds that of cracks is not as extreme as for the comparison with floes. The difference is still large though, and for the parameter range used here it is up to 2.5 orders of magnitude.

An array of 50 m wide ridges will therefore produce greater attenuation than a corresponding array of cracks, until the (base-level) ice becomes thick and/or the wave periods becomes small. Clearly wide ridges will cause more attenuation than narrow ones, and it is natural to ask how the point at which the transition between crack-ridge dominance changes with the ridge width.

The right-hand panel of figure 14 shows the ridge width required for its attenuation coefficient to exceed that of cracks, as a function of wave period and ice thickness. As expected from the results shown in the left-hand panel, it is evident that the required width decreases as the wave period gets larger. However, it also appears that the dependence on period is lost for sufficiently large periods.

For almost half of the spectrum considered, ridges of a 20 m width or less are sufficient to produce greater attenuation than that produced by cracks. As 20 m is a relatively small width for a pressure ridge, it can be inferred that the attenuation produced by ridges is generally more significant than that of cracks. However, note that the minimum width required for ridge attenuation to be greater than crack attenuation changes rapidly for small wave periods. For example, at a 5 s period, although attenuation is greater for a 20 m wide ridge than a crack for thicknesses less than approximately 1.8 m, for thicknesses above approximately 2.5 m a ridge width of 120 m or more is required.

In figure 15 the attenuation produced by floes is compared to the attenuation produced by roughness, as a function of wave period and floe length. Two roughness amplitude and ice thickness combinations are considered: 0.1 m and 1 m, respectively, in the left-hand panel and 0.2 m and 4 m, respectively, in the right-hand panel. The contour values denote the ratio of the dimensional attenuation coefficient for roughness to that for floes, scaled logarithmically.

Positive values therefore indicate that the attenuation produced by rough ice exceeds the attenuation produced by uniform floes, i.e. by scattering produced by the floe edges. However, only negative values are found in both the left-hand and right-hand panels of figure 15, indicating that the attenuation produced by floes dominates over that produced by roughness for these parameter values. The dominance is greatest in the right-hand panel, which may be anticipated, as it has already been noted that floe attenuation increases as ice becomes thicker, whereas roughness attenuation decreases. For the cases considered here the floe attenuation is never less than an order of magnitude greater than roughness attenuation, and the difference is up to 5 orders of magnitude. The roughness amplitudes used here are 10% and 5% of the base-level ice thicknesses, respectively, which are significant proportions. It is therefore concluded that the attenuation due to roughness does not have to be considered in addition to the attenuation produced by floe edges, which is a large numerical advantage.

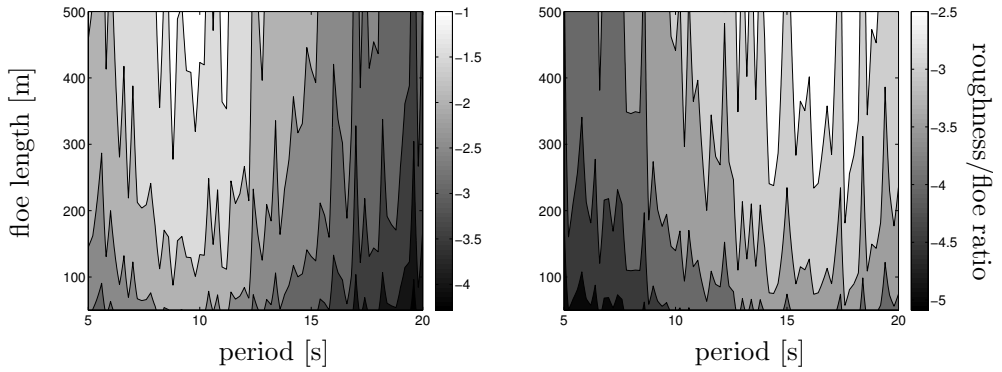

Figure 15: The ratio of the (dimensional) attenuation coefficient for roughness to floes, as a function of wave period and average floe length. The ice thickness is 1 m (left-hand panel) and 4 m (right-hand panel). The roughness amplitude is 0.1 m (left-hand panel) and 0.2 m (right-hand panel), and the roughness unit length is 1 m in both panels. The contour values are on $\log_{10}$ scales.

The ratio of the two attenuation coefficients gets larger as the floe length increases. However, for floe and roughness attenuation to be comparable, generally the floes are so large that the ice cover would be considered as being quasi-continuous. This would only occur deep into the ice pack, and at this point the ice cover is likely to contain cracks and pressure ridges.

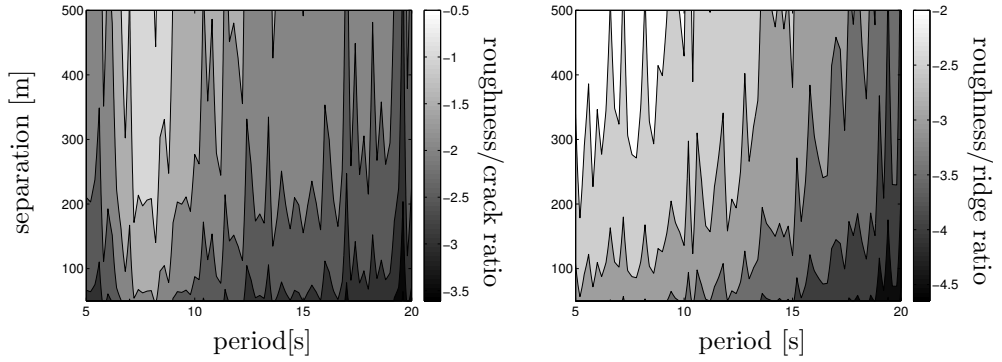

Figure 16: The ratio of the (dimensional) attenuation coefficient for roughness to cracks (left-hand panel) and pressure ridges (right-hand panel), as functions of wave period and average separation. The ice thickness is 1 m (left-hand panel) and 2 m (right-hand panel). The roughness amplitude is 0.1 m (left-hand panel) and 0.2 m (right-hand panel), and the roughness unit length is 1 m in both panels. In the right-hand panel, the ridge width is 50 m. The contour values are on $\log_{10}$ scales.

It then only remains to compare the attenuation produced by roughness to that produced by cracks and pressure ridges. Examples are given in figure 16, for an interval of wave periods and separations of cracks/ridges. The results shown are of the ratio of the dimensional attenuation coefficient for roughness to that for cracks (left-hand panel) and ridges (right-hand panel). In the former the ice thickness is 1 m and the roughness amplitude is 0.1 m. In the latter the ice thickness is 2 m, the roughness amplitude is 0.2 m, and the ridges are 50 m wide.

The results again only display negative values, which indicates that the attenuation produced by cracks/ridges exceeds that produced by roughness for all of the chosen parameter combinations. The closest that the roughness attenuation comes to crack attenuation is half an order of magnitude and for ridge attenuation is 2.5 orders of magnitude. Although the roughness attenuation becomes more significant as the separation of the features increases, the likelihood of finding a highly rough transect of ice with infrequent cracks or pressure ridges is considered low. On the basis of this investigation it is therefore reasonable to disregard the attenuation produced by roughness completely.

5. Summary and conclusions

The reported study was conducted in preparation for the assimilation of wave-ice interactions into an operational model. An investigation was made into the sensitivity of the attenuation created by inhomogeneities in the ice cover through scattering, using an established model. Three features in the ice cover were included in the model, these being floes, cracks and pressure ridges. The attenuation produced by roughness was also considered, this being modelled by a series of small variations in the thickness profile of the sea ice.

The main restrictions of the model are that it assumes linear motions, only allows the geometry to vary in a single spatial dimension and precludes lateral motion of the ice cover. However, it does consider the full multiple scattering problem, including the phases of the waves, which are averaged over all possible values to simulate the randomness of the physical problem. Wave energy reduces exponentially with distance through the ice cover. The rate of exponential decay is defined by an attenuation coefficient, which may be obtained at a low cost using some viable approximations. This is fundamental in allowing for the thorough analysis performed here.

The key findings of this work follow.

1. The value of the Young's modulus used in the model can have a significant effect on the scattering properties of the ice cover. However, the difference in its value for first-year and multi-year ice is not significant.
2. The attenuations produced by floes and cracks are sensitive to the ice thickness and the wave period. Both increase with larger values of the former and smaller values of the latter. Pressure ridges and roughness also produce greater attenuation as the wave period decreases. However, thicker (base-level) ice results in less attenuation from ridges and roughness.
3. The dependence on concentration of floes, cracks and pressure ridges is created in the mapping from the non-dimensional to dimensional attenuation coefficients. Attenuation is therefore inversely proportional to the separation (centre to centre) of adjacent features.
4. The attenuation produced by floes is more sensitive to thickness for smaller wave periods, whereas for cracks the sensitivity is greater for larger wave periods.
5. The reflection produced by an ice edge, and hence the attenuation produced by floes, with respect to ice thickness can be approximated using a hyperbolic tangent. For cracks the non-dimensional attenuation coefficient with respect to ice thickness can be approximated with a power law.
6. The attenuation produced by pressure ridges is most sensitive to the width of the ridge for small wave periods and thin base-level thicknesses, and this sensitivity is approximately quadratic. With respect to base-level thickness, the sensitivity is greatest for small wave periods and for narrow ridges, and is roughly exponential.
7. The attenuation produced by roughness is approximately linear with respect to its unit length and approximately quadratic with respect to its amplitude.
8. Given an array of floes, an array of cracks and an array of ridges, which share identical average separations and ice thicknesses
   (a) The floes will produce more attenuation than the cracks for thin ice and large wave periods, whereas cracks will produce more attenuation if the ice is thicker than approximately 2 m. However, in many circumstances the attenuations will be of the same order of magnitude.

(b) The ridges will generally produce more attenuation than the floes and the cracks, except for thick (base-level) ice and small periods. The difference between ridges and floes or cracks can be very large, especially for floes (4 orders of magnitude in one example shown).

9. The attenuation produced by roughness is generally several orders of magnitude smaller than that produced by floes, cracks or pressure ridges. It is therefore not a significant contributor to scattering-induced attenuation.

The above conclusions are currently being used to construct an optimal look-up table for the operational ice/ocean forecasting model discussed in § 1. Of course, the implementation in the model, in particular the way in which the properties of the ice cover are obtained, still requires careful investigation.

With this work in some sense concluding the study of scattering-induced attenuation of ice-coupled waves in a two-dimensional setting, two main areas are open for future investigation. The first is to model the additional processes that contribute to attenuation and to isolate the regime or regimes in which they are dominant. Secondly, the three-dimensional model must be further developed. It is expected that the motion in the additional dimension will modify the predicted attenuation to some degree. Moreover, it will also allow for an analysis of the directional evolution of the wave field through the ice-covered ocean, which is an important component to incorporate in the operational model.

Acknowledgements

This study is part of Waves-in-Ice Forecasting for Arctic Operators, funded by the Research Council of Norway and Total E&P Norge. The authors are grateful for this support and that of the University of Otago. The authors also thank Dany Dumont, Alison Kohout and Timothy Williams for helpful discussions.

[1] Andreas, E. L., Lange, M. A., Ackley, S. F., Wadhams, P., 1993. Roughness of Weddell Sea ice and estimates of the air-ice drag coefficient. J. Geophys. Res. 98 (C7), 12439–12452.

[2] Bennetts, L. G., 2011. Wave attenuation through multiple rows of scatterers with differing periodicities. SIAM J. Appl. Maths. 71 (2), 540–558.

[3] Bennetts, L. G., Peter, M. A., Squire, V. A., Meylan, M. H., 2010. A three-dimensional model of wave attenuation in the marginal ice zone. J. Geophys. Res. 115, C12043.

[4] Bennetts, L. G., Squire, V. A., 2012. On the calculation of an attenuation coefficient for transects of ice-covered ocean. Proc. R. Soc. Lond. A. 468 (2137), 136–162

[5] Bourke, R. H., McLaren, A. S., 1992. Contour mapping of Arctic basin ice draft and roughness parameters. J. Geophys. Res. 97 (C11), 17715–17728.

[6] Bromirski, P. D., Sergienko, O. V., MacAyeal, D. R., 2010. Transoceanic infragravity waves impacting Antarctic ice shelves. Geophys. Res. Lett. 37 (L02502).

[7] Brunt, K. M., Okal, E. A., MacAyeal, D. R., 2011. Antarctic ice-shelf calving triggered by the Honshu (Japan) earthquake and tsunami, March 2011. J. Glaciol. 57, 785–788.

[8] Cathles, L. M., Okal, E. A., MacAyeal, D. R., 2009. Sea-swell arrival at the front of the Ross Ice Shelf, Antarctica, observed in a 2-year seismometer record. J. Geophys. Res. 114 (F02015).

[9] Dumont, D., Kohout, A. L., Bertino, L., 2011. A wave-based model for the marginal ice zone including a floe breaking parameterization. J. Geophys. Res. 116 (C04001).

[10] Kohout, A. L., Meylan, M. H., 2008. An elastic plate model for wave attenuation and ice floe breaking in the marginal ice zone. J. Geophys. Res. 113: C09016.

[11] Kohout, A. L., Meylan, M. H., Plew, D. R., 2011. Wave attenuation in a marginal ice zone due to the bottom roughness of ice floes. Annals of Glaciology 52 (57), 118–122.

[12] Lange, M. A., Eiken, H., 1991. The sea ice thickness distribution in the northwestern Weddell Sea. J. Geophys. Res. 96 (C3), 4821–4837.

[13] Overgaard, S., Wadhams, P., Lepparanta, M., 1983. Ice properties in the Greenland and Barents seas during summer. J. Glaciol. 29 (101), 142–164.

[14] Squire, V. A., 1993. A comparison of the mass loading and elastic plate models of an ice field. Cold Reg. Sci. Technol. 21, 219–229.

[15] Squire, V. A., 2007. Of ocean waves and sea-ice revisited. Cold Reg. Sci. Technol. 49, 110–133.

[16] Squire, V. A., Dugan, J. P., Wadhams, P., Rottier, P. J., Liu, A. K., 1995. Of ocean waves and sea ice. Annu. Rev. Fluid Mech. 27, 115–168.

[17] Squire, V. A., Moore, S. C., 1980. Direct measurement of the attenuation of ocean waves by pack ice. Nature 283, 365–368.

[18] Timco, G. W., Burden, R. P., 1997. An analysis of the shapes of sea ice ridges. Cold Reg. Sci. Technol. 25, 65–77.

[19] Timco, G. W., Weeks, W. F., 2010. A review of the engineering properties of sea ice. Cold Reg. Sci. Technol. 60, 107–129.

[20] Wadhams, P., Doble, M. J., 2008. Digital terrain mapping of the underside of sea ice from a small AUV. Geophys. Res. Lett. 35, L01501.

[21] Wadhams, P., Squire, V. A., Goodman, D. J., Cowan, A. M., Moore, S. C., 1988. The attenuation rates of ocean waves in the marginal ice zone. J. Geophys. Res. 93 (C6), 6799–6818.

[22] Williams, T. D., Squire, V. A., 2002. Wave propagation across an oblique crack in an ice sheet. Int. J. Offshore Polar Eng. 12 (3), 157–162.